SCIENTIFIC REP⚙RTS

Enhanced photovoltaic properties in dye sensitized solar cells by surface treatment of SnO$_2$ photoanodes

Kaustubh Basu[1], Daniele Benetti[1], Haiguang Zhao[1], Lei Jin[1], Fiorenzo Vetrone[1,4], Alberto Vomiero[2] & Federico Rosei[1,3,4]

We report the fabrication and testing of dye sensitized solar cells (DSSC) based on tin oxide (SnO$_2$) particles of average size ~20 nm. Fluorine-doped tin oxide (FTO) conducting glass substrates were treated with TiO$_x$ or TiCl$_4$ precursor solutions to create a blocking layer before tape casting the SnO$_2$ mesoporous anode. In addition, SnO$_2$ photoelectrodes were treated with the same precursor solutions to deposit a TiO$_2$ passivating layer covering the SnO$_2$ particles. We found that the modification enhances the short circuit current, open-circuit voltage and fill factor, leading to nearly 2-fold increase in power conversion efficiency, from 1.48% without any treatment, to 2.85% achieved with TiCl$_4$ treatment. The superior photovoltaic performance of the DSSCs assembled with modified photoanode is attributed to enhanced electron lifetime and suppression of electron recombination to the electrolyte, as confirmed by electrochemical impedance spectroscopy (EIS) carried out under dark condition. These results indicate that modification of the FTO and SnO$_2$ anode by titania can play a major role in maximizing the photo conversion efficiency.

Over the last two decades, dye sensitized solar cells (DSSCs) have been widely explored as potential alternatives to conventional silicon photovoltaic (PV) devices due to their low cost, abundance of raw material, facile fabrication process and overall good photovoltaic performance (record efficiency above 14%)[1,2]. Compared to typical semiconductors used in p-n junction solar cells, the materials employed in a DSSC photoanode may have lower purities[3], thereby leading to lower production costs[4,5]. However, to become a realistic candidate to replace traditional solar cells, several challenges have to be addressed to enhance device performance. The photoanode material plays a major role for such purposes: TiO$_2$ nanoparticle films have been widely used in DSSCs, thanks to the very fast electron injection rates from the excited state of the dye into the TiO$_2$ nanoparticle conduction band, of the order of femtoseconds. On the other hand, due to limited electron mobility in TiO$_2$, the high electron recombination rate leads to degradation of photoconversion efficiency (PCE)[6].

Other potentially suitable semiconducting metal oxides were recently considered, such as ZnO and SnO$_2$[7–10]. These are appealing candidate materials, due to their higher electron mobility, as compared to TiO$_2$[11,12] and specific advantages, such as: (i) the ZnO band gap and band positioning is energetically similar to TiO$_2$[1]; (ii) SnO$_2$ on the other hand is a promising oxide material because of its higher electronic mobility and large band gap (3.8 eV)[13]. The mobilities reported in both single crystal SnO$_2$[14] as well as nanostructures[15] are orders of magnitude higher than in single crystal TiO$_2$[6]. The high electron mobility in SnO$_2$ compared to its counterpart TiO$_2$, leads to faster diffusion-mediated transport of photoinjected electrons. The wider bandgap of SnO$_2$, compared to anatase TiO$_2$ (3.2 eV) creates fewer oxidative holes in the valence band under UV illumination, so as to minimize dye degradation rate and long term stability of DSSCs[16,17]. Because of these appealing properties, SnO$_2$ has been recently utilized in other advanced applications[18–20], including hydrogen gas sensing[21,22]. Various synthesis

[1]Institut National de la Recherche Scientifique-Énergie, Matériaux et Télécommunications, Université du Québec, Varennes, QC, Canada. [2]Department of Engineering Sciences and Mathematics, Luleå University of Technology, 971 98, Luleå, Sweden. [3]Institute for Fundamental and Frontier Science, University of Electronic Science and Technology of China, Chengdu 610054, P.R. China. [4]Centre for Self-Assembled Chemical Structures, McGill University, Montreal, QC, Canada. Correspondence and requests for materials should be addressed to A.V. (email: alberto.vomiero@ltu.se) or F.R. (email: rosei@emt.inrs.ca)
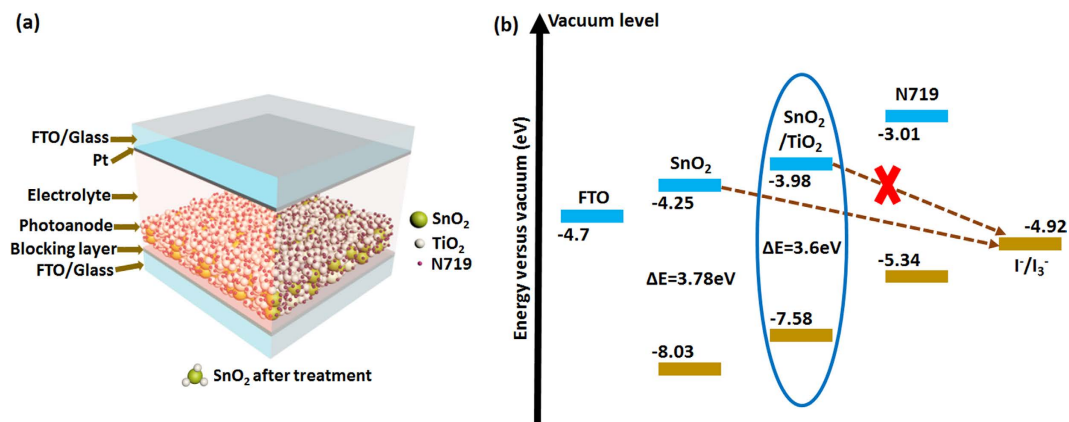
Figure 1. (**a**) Proposed schematic representation of DSSC. (**b**) Electronic band diagram showing the beneficial effect of the present methodology to modify SnO_2 anode by TiO_2 (encircled) in alleviating charge recombination from anode to electrolyte as opposed to only using SnO_2 anode. The conduction band, valence band positions and band gap values of present SnO_2 anode and SnO_2 anode modified by TiO_2 are calculated from data acquired from the combination of UPS and diffuse reflectance spectroscopy. All other values are from reported literature[61–63].

techniques of SnO_2 nanocomposites have also been reported in recent literature[23,24]. In the specific field of DSSCs, a drawback of SnO_2 is its faster electron recombination kinetics and lower trapping density compared to TiO_2, resulting from a 300 mV positive shift of conduction band relative to TiO_2, which results in an increased dark current, thereby limiting the open circuit voltage[25,26]. In addition, SnO_2 has a lower isoelectric point (IEP, at pH 4–5) than anatase TiO_2 (IEP at pH 6–7)[27], which leads to lower dye adsorption with acidic carboxyl groups[26], decreasing the optical density of the photoanode and its ability to absorb solar radiation. In DSSCs, the FTO glass can directly come in contact with the electrolyte, since the mesoporous photoanode cannot uniformly cover the entire FTO surface. At the FTO-electrolyte interface, charge recombination limits electron collection and affects PCE[28–32]. Modification of the FTO/electrolyte interface plays a key role in boosting DSSC performance by suppressing the recombination of electrons from the FTO to the electrolyte. A promising approach for such interface modification is to add a compact metal oxide blocking layer on FTO that would inhibit back electron transport from FTO to the electrolyte[33]. Also, TiO_2-SnO_2 based heterojunctions can be potentially considered to mitigate the problem of low electron mobility in TiO_2 and fast electron recombination in SnO_2. In fact, the conduction band edge of SnO_2 is at a lower position than that of TiO_2, so the electrons injected from the dye to TiO_2 can be efficiently injected into SnO_2, which in turn also has a higher mobility, so that the overall electron conductivity of the system can be enhanced[13]. The TiO_2-SnO_2 heterojunction creates a cascading band structure when layered with the N719 dye[34,35]. Recently, a new record conversion efficiency around 7.4% has been set with SnO_2 multiporous nanofibers DSSC with $TiCl_4$ treatment by Qamar Wali and co-workers[19]. Multistep electron transport down a cascading band structure increases carrier lifetime and reduces charge recombination[36]. Also, a thin TiO_2 passivating layer at the surface of SnO_2 nanoparticles can reduce recombination of electrons from the SnO_2 photoanode to the electrolyte, which is one of the main contributors that cause poor performance of SnO_2 solar cells.

In this manuscript, we implement a modified SnO_2 photoanode, in which the concept of efficient electron injection is pursued in a SnO_2-TiO_2 heterojunction (Fig. 1), to form a cascading band structure[34,35] by modifying the SnO_2 photoanode with $TiCl_4$ or TiO_x precursor solution, and treating the FTO substrates with the same precursor solutions to form a blocking layer. The morphological characterization of the photoanode indicates an interconnected structure of SnO_2 and TiO_2 nanoparticles, where small TiO_2 nanoparticles grow on top of each other forming wire-like structures connecting the mesoporous SnO_2 photoanode. The functional characterization of the entire solar cell (which demonstrate a marked improvement of photovoltaic parameters) indicated an overall increase of ~90% in the PCE from 1.48% without any treatment, to 2.85% achieved with $TiCl_4$ treatment.

Results and Discussion

Size tuning of nanoparticles is very important in determining the performance of DSSCs. The optimum size is around 20 nm, because for larger nanoparticles, less surface per unit volume is available for dye adsorption. On the other hand, in the case of smaller sized nanoparticles, a larger number of grain boundaries can be found, which increases the probability of electron trapping[37–40], and smaller pore size, which can inhibit dye penetration during the sensitization process[41]. We chose SnO_2 nanoparticles ~20 nm in diameter for photoanode preparation. The surface morphology of different photoanodes, with/without treatment is illustrated in Fig. 2(a–d). The typical mesoporous structure is visible after sintering. The $TiCl_4$ treatment (Fig. 2b,c) induces the formation of small nanoparticles of about 5 nanometers (nm), which are confirmed to be composed of titanium oxide by energy dispersive X-ray spectroscopy (EDX) selectively performed on a single nanoparticle, as shown in Fig. 3. The TiO_2 nanoparticles preferentially form short interconnected nanowires (Fig. 2b,c). The higher the $TiCl_4$ molar concentration, the more connected is the wire-like structure (see comparison of Fig. 2b,c and Fig. 2f,g). The TiO_x treatment induces the formation of completely different structures compared to $TiCl_4$: the TiO_x structures seem to cover the larger SnO_2 particles. If we compare the scanning electron microscope (SEM) and transmission electron
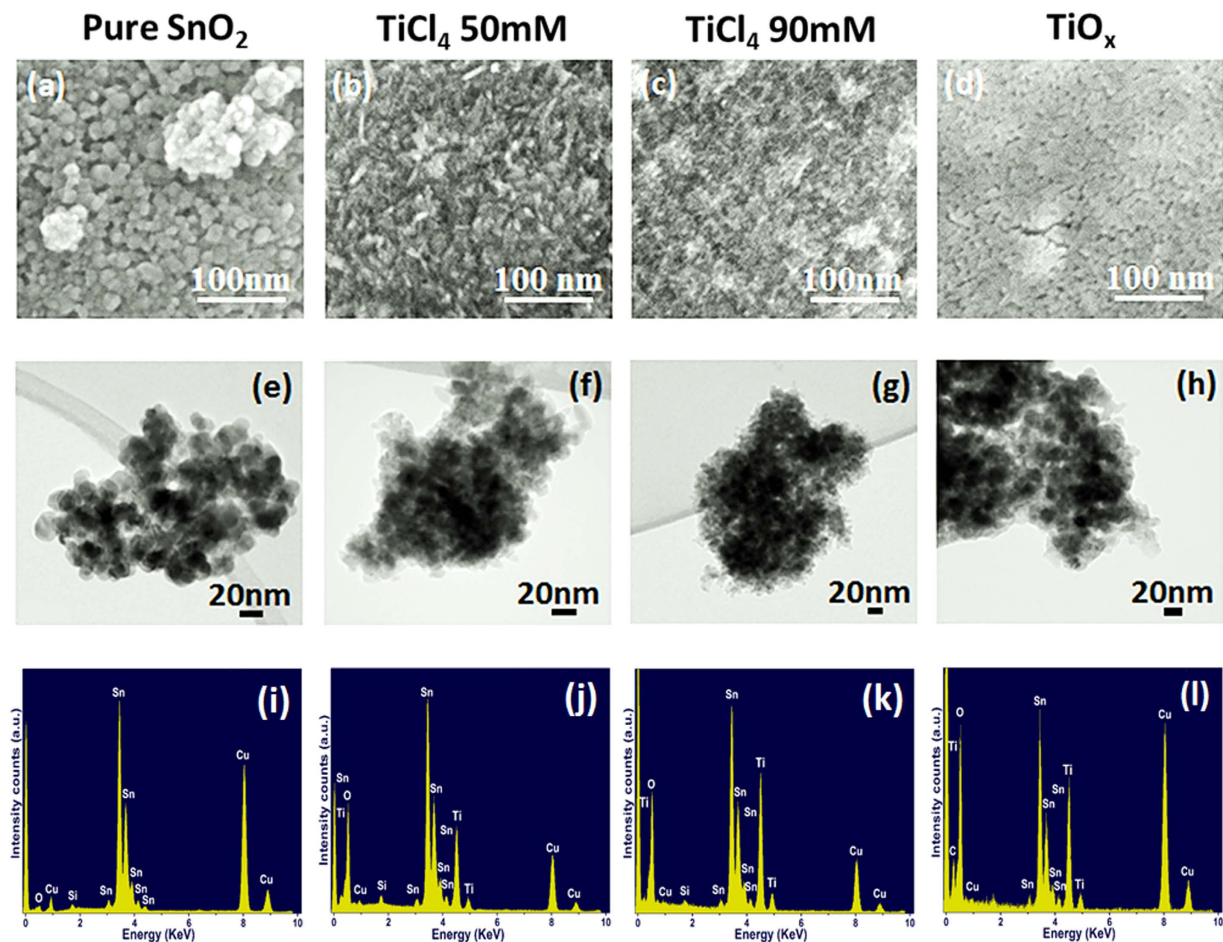
Figure 2. SEM images (**a–d**), TEM images (**e–h**), and EDX spectra (**i–l**) on different SnO$_2$ photoanodes, confirming the presence of the constituent elements, SnO$_2$ anodes: (**a,e,i**) before treatment; (**b,f,j**) treated with 50 mM TiCl$_4$; (**c,g,k**) treated with 90 mM TiCl$_4$; (**d,h,l**) treated with TiO$_X$.
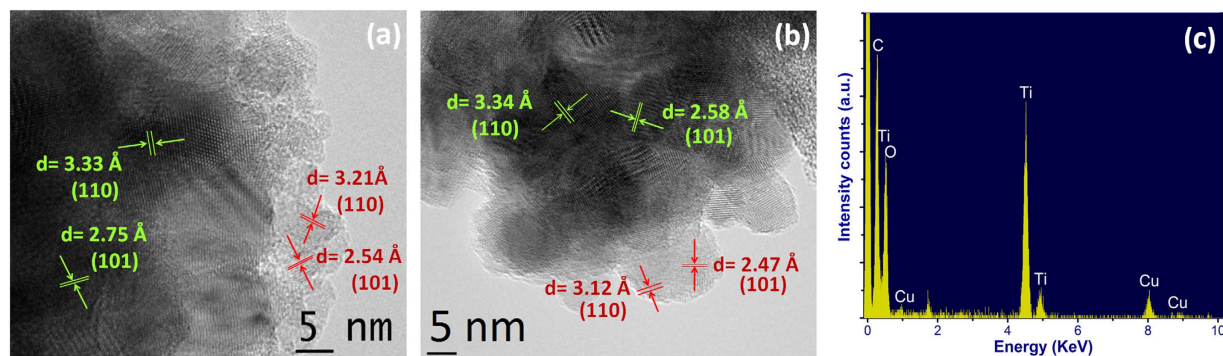

Figure 3. HRTEM images of (**a**) TiCl$_4$ treated and (**b**) TiO$_x$ treated SnO$_2$ nanoparticles. (**c**) EDX spectra confirming the presence of constituent elements of TiO$_2$ when selectively done on the TiO$_2$ nanoparticles covering the SnO$_2$ nanoparticles, the presence of Cu and C is due to the grid used as sample holder.

microscope (TEM) images from Fig. 2, we can more clearly observe the influence of the different precursors on bare SnO$_2$ nanoparticles. Inspection of TEM images reveal that the pure SnO$_2$ sample consists of spherical nanoparticles whose average size is about 20 nm (Fig. 2e). However, TEM images Fig. 2f through Fig. 2h indicate that spherical nanoparticles of size around 20 nm are decorated with smaller size nanoparticles, which sometimes grow on top of one another to form nanowire like structures (SEM images 2b and 2c) and sometimes cover the SnO$_2$ nanoparticles (Fig. 2d). EDX mapping analysis is reported in Fig. 2. The elemental characterization of the SnO$_2$ photoanode is shown in Fig. 2i. EDX carried out on SnO$_2$ mesoporous photoanode treated with 50 mM
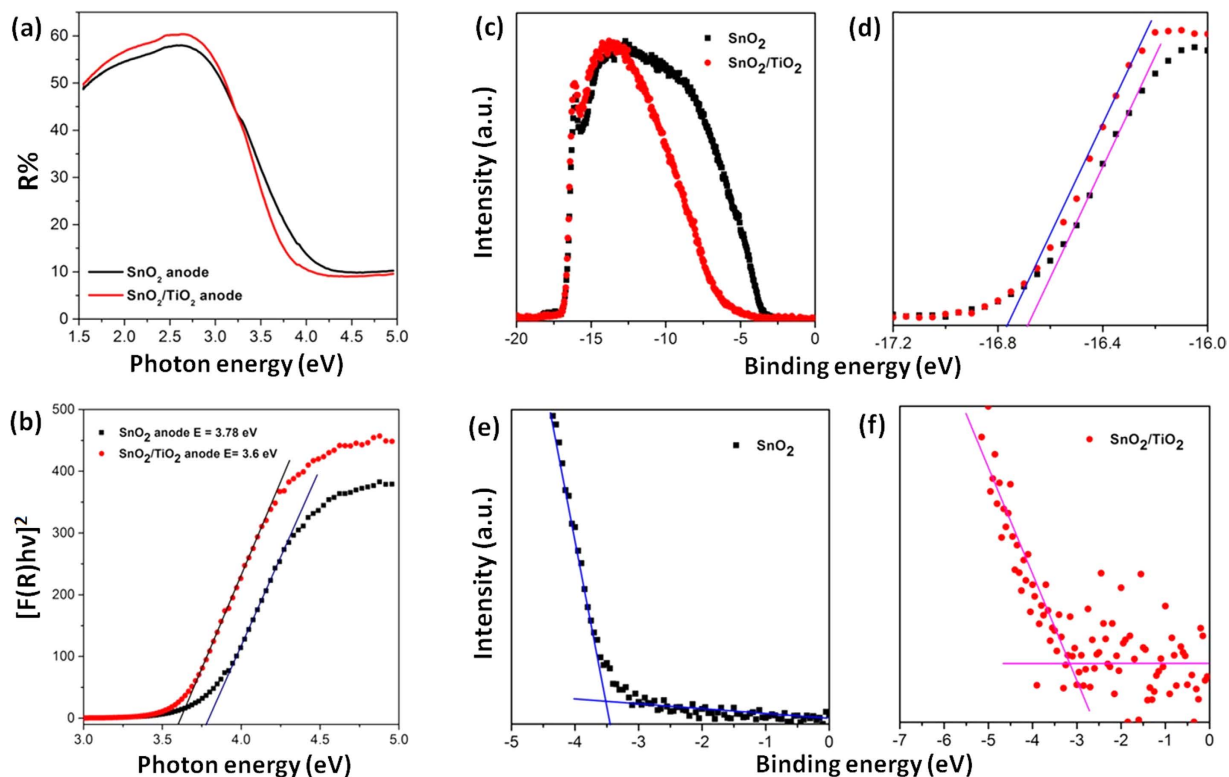
Figure 4. (**a**) Diffuse Reflectance spectra plotted with respect to photon energy for SnO_2 anode and SnO_2 anode after TiO_x post-treatment; (**b**) Kubelka-Munk transformed spectra for SnO_2 anode and SnO_2 anode after treatment; (**c**) Complete UPS of SnO_2 and treated SnO_2 anodes; (**d**) magnified view of high binding energy cut-off (Fermi level) and (**e,f**) low binding energy cut-off (VB edge) of SnO_2 anode and SnO_2 anode after TiO_x post-treatment respectively.

$TiCl_4$, 90 mM $TiCl_4$ and TiO_X are shown in Fig. 2j, k and l, repectively and confirm the presence of the constituent elements of SnO_2 and TiO_2. High Resolution Transmission Electron Microscopy (HRTEM) was carried out on treated samples to examine their fine structure. The results are reported in Fig. 3, which shows the crystalline structure of the SnO_2 and the TiO_2 nanoparticles. Distinct lattice fringes in the HRTEM images highlight the presence of crystalline phases for both SnO_2 (green coloured text) and TiO_2 (red coloured text). HRTEM indicates that the crystalline phase of both SnO_2 and TiO_2 can be indexed to a rutile structure, (JCPDS No. 00-041-1445 and JCPDS No. 01-088-1175, respectively). This finding is consistent for both $TiCl_4$ and TiO_x treatments. X-ray diffraction (XRD) analysis was performed to further confirm the crystalline structure of our anodes and is reported in Fig. S1. In all the cases the diffraction pattern matches with rutile SnO_2 (JCPDS No. 00-041-1445). XRD reveals that the crystal structure of SnO_2 nanoparticles did not change after TiO_x treatment or after the photoanalysis process. TiO_2 peaks could not be found for the treated samples since the quantity is most likely below the detection limit.

To determine the band gap of SnO_2 photoanode before and after post-treatment, diffuse reflectance spectroscopy measurement were carried out. Kubelka Munk function was used to calculate the band gap of SnO_2 photoanode before and after TiO_x post-treatment (Fig. 4). The band gap of SnO_2 photoanode was found to be 3.78 eV, which is consistent with literature[37] and the band gap of SnO_2 photoanode after TiO_x post-treatment was found to be 3.6 eV. Ultraviolet Photoelectron spectroscopy (UPS) analysis (Fig. 4c–f), was performed to identify the band positions of the various photoanodes. The valence band (VB) edge for SnO_2 anode is -8.03 eV, which shifts to a higher value of -7.58 eV after TiO_x post-treatment. The energy band gap values from Kubelka-Munk transformed diffuse reflectance spectra for SnO_2 anode and SnO_2 anode after TiO_x post-treatment along with values of valence band edge from UPS measurement reveals the lowest position of the conduction band (CB) for both the samples. The values of CB minima, VB maxima, and the band gap for SnO_2 anode and SnO_2 anode after TiO_x post-treatment are reported in Fig. 1b. X-ray photoelectron spectroscopy analysis (XPS), was performed to detect any possible shift in the binding energy for the Ti 2p and Sn 3d peaks. The high resolution XPS of Ti 2p of the treated anode and the treated anode after photoanalysis process (Fig. S2) shows that there is no significant change for Ti 2p peaks after the cell operation, which means that the chemical state of Ti^{4+} does not change during the photoanalysis process. Similar inference can be also drawn in the case of Sn 3d peaks, which are reported in Fig. S3, confirming that the chemical state of Sn^{4+} does not change.

To understand the influence of the different treatments on the cell performance, the functional properties of the solar cells were investigated under standard AM1.5G simulated sun irradiation. The results are presented in Fig. 5, and the PV parameters (open circuit voltage (V_{oc}), short circuit photocurrent density (J_{sc}), fill factor (FF),
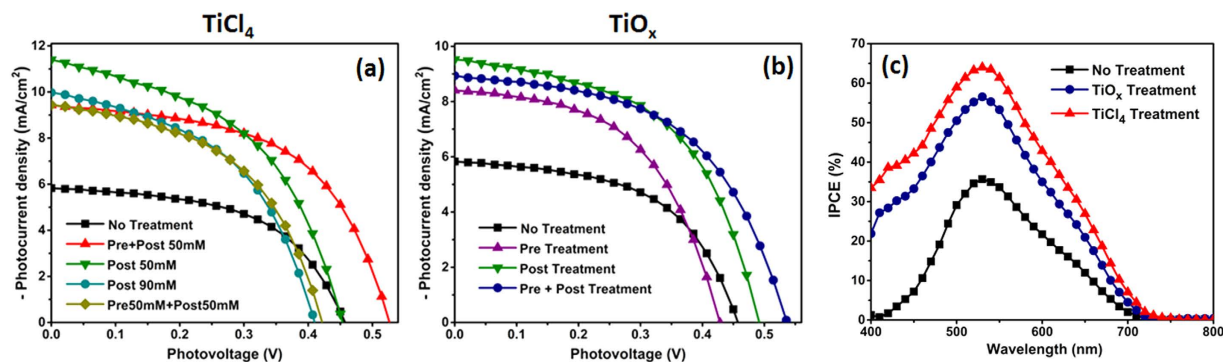
Figure 5. (**a**) Photocurrent density–photovoltage (J-V) characteristics of SnO_2 nanoparticle based DSSCs, under 1 Sun illumination, obtained from pre- and post-treatment of different concentration of $TiCl_4$ precursor; (**b**) J-V characteristics obtained from pre- and post-treatment of TiO_x precursor; (**c**) Dependence of absolute IPCE of the solar cells with dye-sensitized SnO_2 nanoparticle electrodes modified with TiO_X and $TiCl_4$ tretament.

DSSC	Treatment type	V_{oc} (V)	J_{sc} (mA/cm^2)	Fill Factor (FF)	Efficiency (%)
SnO_2_1	No Treatment	0.45	5.83	0.56	1.48
$TiCl_4$_1	$TiCl_4$ Pre 50 mM + Post 50 mM	0.53	9.43	0.57	2.85
$TiCl_4$_2	$TiCl_4$ Pre 50 mM + Post 90 mM	0.43	9.44	0.53	2.15
$TiCl_4$_3	$TiCl_4$ Post 50 mM	0.45	11.4	0.51	2.64
$TiCl_4$_4	$TiCl_4$ Post 90 mM	0.41	9.98	0.52	2.13
TiO_x_1	TiO_x Pre Treatment	0.43	8.41	0.54	1.96
TiO_x_2	TiO_x Pre + Post Treatment	0.53	8.94	0.56	2.66
TiO_x_3	TiO_x Post Treatment	0.49	9.52	0.55	2.59

Table 1. Photovoltaic properties of DSSC with different configurations of TiO_x and $TiCl_4$ treatment.

and PCE) are shown in Table 1.A maximum PCE of 2.85% is achieved in the $TiCl_4$-treated cell (with pre- and post-treatment) and 2.66% for TiO_x pre- and post-treatment, compared to 1.48% for the pristine SnO_2 photoanode. This marked improvement in the PCE originates from the higher V_{oc} and J_{sc} of the cells, which in turn are induced by the treatments. A possible explanation in the increase of V_{oc} can be due to an increase of electron density in SnO_2 as a consequence of effectively suppressed recombination, the Fermi level shifts to a more negative value[42] and since V_{oc} is the difference between the Fermi level in the semiconductor and the redox potential of I–/I^{3-} of the electrolyte, a higher value of open circuit voltage is recorded for all treated anodes. A high V_{oc} of 0.53 V can be observed for the best $TiCl_4$ and TiO_x treated cells. Also due to the treatment, the electronic contact between the nanoparticles is improved because of broadened contact interface and the increased contact point which make the electrons traverse the film more easily[43], which further confirms the reduction of recombination. In addition, interconnection between the nanoparticles facilitate the percolation of electrons from one nanoparticle to other and lead to a global increase of current[43]. However, when we introduce additional TiO_2 by treating our anodes with higher molar concentration of $TiCl_4$, due to the increase in nucleation and growth of nanoparticles, which leads to higher concentration and density of the nanoparticles, there is a reduction of film porosity, which may lead to a decrease of dye adsorption, thus deteriorating the PV properties[44,45]. For $TiCl_4$ modification, the J_{sc} increases by ~60% from the untreated cell and for TiO_x modification, an increase of 53% is observed. The family of IPCE curves in Fig. 5 are constructed with the IPCE spectra of a normal SnO_2 photoanode cell and the best cells with both TiO_x and $TiCl_4$ treatment. The curves are in accordance with the current density versus voltage curves where we observe a marked improvement as a result of treatment. As already established from SEM images, in case of $TiCl_4$ treatment, the small titania nanoparticles connect with each other, forming nanowire like structures. On the other hand, in the case of TiO_x treatment, TiO_2 particles cover the SnO_2, effectively reducing direct contact of SnO_2 with the electrolyte, possibly decreasing recombination, thereby leading to an enhancement of IPCE.

We performed electrochemical impedance spectroscopy (EIS) analysis to understand the physical-chemical processes which regulate charge dynamics in our cells. Fig. 6 displays the EIS spectra under dark condition of our pristine SnO_2 cell and the two best cells after $TiCl_4$ and TiO_x treatments. The treated cells were subjected to a pre-treatment that forms a blocking layer (BL) and a post-treatment that influenced film morphology and PV performances[3,46,47]. The role of the BL in DSSCs is still under debate; different hypotheses have been formulated. Cameron and Peter, and more recently Park and co-workers demonstrated the ability of the BL to prevent back reaction (i.e. electron recombination from FTO to electrolyte) of electrons and attributed the improved performance to the charge transfer resistance at the BL/electrolyte interface. Hence, BL was effective in reducing charge losses at the FTO/anode interface[48,49]. On the other hand, Fabregat and co-workers indirectly deduced that the main factor leading to the enhancement in PCE was the improved physical contact between the coated FTO and
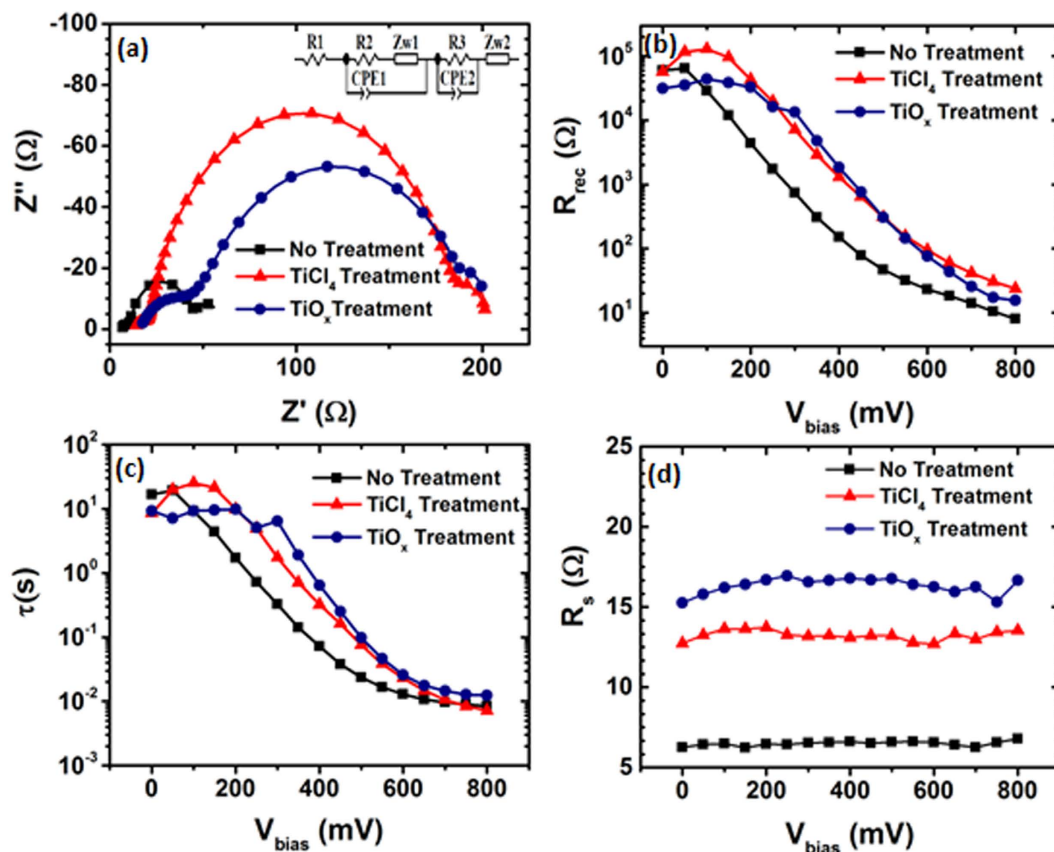
Figure 6. (a) Nyquist plots of devices with and without treatment, under dark condition and around V_{oc}. The inset shows the model used for fitting the data. From left to right of the model in the inset: series resistance (R1), electron transport and back reaction at the TiO_2/electrolyte interface, charge transfer at electrolyte/Pt-FTO interface and diffusion of ions in the electrolyte. **(b)** Recombination resistance as calculated from EIS analysis. **(c)** Electron lifetime obtained from the product $R_{rec}*C_\mu$. **(d)** Series resistance calculated from EIS analysis.

the TiO_2 film[50]. Fig. 6a compares the Nyquist plots of three different cells (bare SnO_2, $TiCl_4$ and TiO_x treatment) under dark condition and at bias voltage equals to V_{oc}. Three semicircles are clearly visible: the high frequency arc is attributed to the redox reaction at the platinum counter electrode, the medium arc takes in account the oxide/electrolyte interface and the low frequency arc is related to the Nerst diffusion in the electrolyte[51,52]. The medium arc is evidently larger for the treated cells, indicating that the methods used, increase the resistance, thus lowering the recombination processes at the oxide/electrolyte interface. Fig. 6b shows the trend of the recombination resistance (R_{rec}) as a function of applied bias. For both treatments, the values of R_{rec} are increased compared to the pristine cell, thus indicating reduced recombination after treatment. The overall trend of R_{rec} clearly shows that after the treatment, the recombination resistance is increased across the whole bias range, confirming a decrease in recombination phenomena. The region at low bias (below ~250 mV) is dominated by the charge recombination and capacitance of the back layer[53,54]. In this region it is thus possible to observe the different contributions to the recombination resistance due to different back layer (in fact, with and without the blocking layers, the response of the system will be different: without BL, increased FTO/electrolyte back reaction occurs)[48,55]. In our case, we can observe that R_{rec} increases, in particular for the $TiCl_4$ treatment, indicating the effectiveness of the BL to reduce charge recombination at this interface. The increase in R_{rec} for TiO_x treatment is lower compared to the $TiCl_4$, probably due to presence of more voids in the blocking layer, which allow the electrolyte to come in contact with the FTO[56].

In general, the combined effect of the pre- and post-treatment on the cells is an increase of the electrons lifetime, as shown in Fig. 6c: the lifetime is systematically higher for the treated cells. Similar results can be found in the literature where the presence of the BL suppresses the charge recombination at the FTO/electrolyte interface[49,57,58]. The main contribution of the post treatment is more difficult to observe in the EIS spectra, because this kind of treatment usually affects the morphology of the sample, modifying, for example, the total surface area. This in turn favors a higher dye loading and greater light harvesting[46], yet has less influence on the electronic processes related to charge transport and recombination. As already found by Fabregat and co-workers, the treated cells present a higher value of the series resistance (R_s) in Fig. 6d, which is detrimental for the overall PCE of the cell[50]. However, this effect is largely compensated by a much higher reduction of the charge recombination at the FTO/electrolyte interface, so that the net result is the enhancement of PCE.

Conclusions and Perspectives

In summary, we demonstrated the synthesis of SnO_2 photoelectrodes prepared with SnO_2 nanoparticles of average size 20 nm, treated with $TiCl_4$ precursor solution and TiO_x flat film precursor solution. The modified photoanodes exhibit a significant relative increase in power conversion efficiency of the solar cell, which is attributed to the enhancement of functional properties of the DSSC. The blocking layer inhibits the transport of electrons back to the electrolytes, which are collected by the FTO, while passivation of the SnO_2 mesoporous layer blocks the back-reaction pathway of photoinjected electrons from semiconductor anode to electrolyte. The enhancement of open circuit voltage was made possible due to the modification of the electronic band alignment because of the reduced charge recombination. The effect of interconnection of the electrode nanoparticles provide a better path for electron flow and plays a major role in enhancing the short circuit current of the device. The increase of R_{rec}, and higher lifetime for solar cells with treated anodes further confirms reduced recombination and greater diffusion length of an electron before recombination, thus enhancing the functional properties of the DSSC, which led to nearly a 2-fold improvement in overall PCE.

We obtained experimental evidence (through UPS and diffuse reflectance) of the possibility to modify the electronic band structure in SnO_2 photoanodes, which facilitates efficient electron transport in treated photoanodes, by suppressing charge recombination and thus improving the functional properties of the DSSC.

Experimental Methods

Preparation of SnO₂ paste. The SnO_2 powder used consists of nanoparticles of average particle size ~20 nm (American Elements 99.9% tin(IV) oxide). 1 g SnO_2 powder was mixed with 5 ml ethanol as a solvent, 1 ml alpha-terpineol as dispersant, 0.5 g ethyl cellulose which acts as a thickener and 1 ml of water. The mixing of these ingredients were carried out in a beaker under overnight magnetic stirring. The solvent was removed by connecting it to a pump while continuous magnetic stirring until the volume of the mixture reduced to half of the starting volume.

Pre- and post-treatment of the SO₂ photoanode. The pre-treatment of the SnO_2 photoanode, i.e. a blocking layer with TiO_2 was deposited by spin coating the TiO_x flat film precursor solution at 2,000 r.p.m. for 60 s and subsequently heating at 500 °C for 30 min[59]. Alternatively, pre-treatment was also carried out by soaking the FTO substrates in 50 mM $TiCl_4$ aqueous solution and 90 mM $TiCl_4$ aqueous solution for 30 min at 70 °C, then they were flushed with deionized water and sintered at 450 °C for 30 min[3]. For post treatment of the SnO_2 film, the same procedure as pretreatment was followed with the TiO_x and $TiCl_4$ precursor solutions.

Diffuse reflectance spectroscopy. Diffuse reflectance spectroscopy of SnO_2 photoanode, and SnO_2 photoanode treated with TiO_x flat film precursor solution was carried out using UV-Visible-NIR spectrometer, Perkin Elmer, Lambda 750 in the wavelength range of 250–800 nm with resolution of 2 nm. Kubelka Munk (K-M) function, was calculated following literature procedure[60], and was plotted as a function of photon energy. K-M function was used to determine the band gap of SnO_2 photoanode before and after post-treatment.

Ultraviolet Photoelectron Spectroscopy. SnO_2 photoanode, and SnO_2 photoanode treaed with TiO_x precursor solution were studied with Ultraviolet Photoelectron Spectroscopy (UPS) collected using VG ESCALAB 3 Mark II high vacuum system. During the UPS measurement, illumination at 21.21 eV was provided by the He (I) emission line from a helium discharge lamp. Cutoff energies were determined from the intersection of a linear extrapolation of the cutoff region to a linear extrapolation of the baseline.

DSSC assembly. Fluorine doped tin oxide (FTO) coated glass substrates (Pilkington, bought from Hartford Glass Co. Inc., USA) with sheet resistance 15 Ω/□ were sonicated for 30 min with 2% Triton X-100 in deionized water to remove traces of glue from packaging, then they were cleaned by 30 min sonication in isopropyl alcohol and then thoroughly rinsed with deionized water and dried in a filtered air stream. Subsequently a blocking layer with TiO_2 was deposited using the techniques described above. Then, a layer of the prepared SnO_2 paste was deposited using a simple doctor blade technique and dried in air for 10–15 min and then fired on a hot plate at 150 °C for 6 min. When the substrates cooled down, another layer was doctor bladed, followed by annealing at 500 °C for 30 min in air and then cooled back to room temperature. Then the SnO_2 film was coated with a passivating layer of TiO_2 by methods described already in the experimental methods section of Pre- and Post-Treatment of the SnO_2 Photoanode. The treated anodes were then sensitized by dye, upon immersion in a 0.5 mM ethanolic solution of the commercial N719 dye (Ruthenizer 535-bisTBA from Solaronix) for 18 h and then washed with ethanol to remove any excess of unabsorbed dye molecules. Solar cells were assembled using a sputtered 10 nm thick platinized counter electrode on FTO glass substrate, 25 μm thick spacer Meltonix 1170-25 (to prevent the cell from short circuiting when the working and counter electrodes are clamped together), and iodide/tri-iodide redox couple HI-30as the electrolyte.

PV measurements. Photocurrent density-voltage (J-V) characteristics were measured under simulated sunlight (1 sun = AM 1.5 G, 100 mW/cm^2) using a Class AAA Solar Simulator from Photo Emission Tech (SS50AAA) with a Keithley 2400 sourcemeter. The simulator used has a class as per ASTM E927, AAA with non-uniformity of Irradiance of 2% or lower over 2 × 2 inch area. The system for device characterization was calibrated with a Si reference diode. The sourcemeter was controlled by a computer using an application written under TESTPOINT software platform. The fill factor (FF) and the power conversion efficiency (PCE) were calculated from the following equations[2].

$$FF = \frac{P_{max}}{J_{sc} \times V_{oc}} = \frac{J_{max} \times V_{max}}{J_{sc} \ X \ V_{oc}} \tag{1}$$

$$PCE(\%) = \frac{P_{max}}{P_{in}} \times 100\% = \frac{J_{sc} \times V_{oc} \times FF}{P_{in}} \times 100\% \tag{2}$$

where P_{max} is the maximum power output, J_{sc} is the short-circuit current density, V_{oc} is the open-circuit voltage, J_{max} is the current density and and V_{max} is the voltage at maximum power output in the J-V curves, and P_{in} is the incident light power.

For the external quantum efficiency (EQE) or incident photon to current efficiency (IPCE) measurements of our devices, we used the Oriel IQE-200 certified system, which is calibrated using NREL certified Si and Ge detectors. The solar cells were connected using a probe station.

EIS measurements.   Electrochemical impedance spectroscopy (EIS) was studied under dark ambience using a SOLARTRON 1260A Impedance/Gain-Phase Analyzer. All spectra were collected by applying an external bias between 0 and 800 mV, in the 100 mHz-300 kHz frequency range. The measurements were carried out inside a Faraday cage for all the samples.

Materials characterization.   The morphology of the samples were studied using Scanning Electron Microscopy (SEM) and Transmission Electron Microscopy (TEM). SEM images were recorded using JEOL JSM840 at an accelerating voltage of 10 kV. Bright field TEM and high resolution HR-TEM imaging at 200 kV and energy dispersive X-ray spectroscopy (EDS) were carried out using JEOL JEM-2100F.

References

1. Gratzel, M. Photoelectrochemical cells. *Nature* **414,** 338–344, doi: 10.1038/35104607 (2001).
2. Hagfeldt, A., Boschloo, G., Sun, L., Kloo, L. & Pettersson, H. Dye-Sensitized Solar Cells. *Chem. Rev.* **110,** 6595–6663, doi: 10.1021/cr900356p (2010).
3. Sommeling, P. M. *et al.* Influence of a $TiCl_4$ Post-Treatment on Nanocrystalline TiO_2 Films in Dye-Sensitized Solar Cells. *J. Phys. Chem. B* **110,** 19191–19197, doi: 10.1021/jp061346k (2006).
4. Späth, M. *et al.* Reproducible manufacturing of dye-sensitized solar cells on a semi-automated baseline. *Progress in Photovoltaics: Research and Applications* **11,** 207–220, doi: 10.1002/pip.481 (2003).
5. Kroon, J. M., O'Regan, B. C., van Roosmalen, J. A. M. & Sinke, W. C. *Handbook of Photochemistry and Photobiology.* Vol. Dye-sensitized solar cells. Inorganic photochemistry 1–47 (American Scientific, 2003).
6. Hendry, E., Koeberg, M., O'Regan, B. & Bonn, M. Local field effects on electron transport in nanostructured TiO_2 revealed by terahertz spectroscopy. *Nano Lett.* **6,** 755–759, doi: 10.1021/nl0600225 (2006).
7. Concina, I. & Vomiero, A. Metal Oxide Semiconductors for Dye- and Quantum-Dot-Sensitized Solar Cells. *Small* **11,** 1744–1774, doi: 10.1002/smll.201402334 (2015).
8. Memarian, N. *et al.* Hierarchically Assembled ZnO Nanocrystallites for High-Efficiency Dye-Sensitized Solar Cells. *Angew. Chem. Int. Ed.* **50,** 12321–12325, doi: 10.1002/anie.201104605 (2011).
9. Fukai, Y., Kondo, Y., Mori, S. & Suzuki, E. Highly efficient dye-sensitized SnO_2 solar cells having sufficient electron diffusion length. *Electrochem. Comm.* **9,** 1439–1443, doi: 10.1016/j.elecom.2007.01.054 (2007).
10. Katoh, R. *et al.* Efficiencies of Electron Injection from Excited N3 Dye into Nanocrystalline Semiconductor (ZrO_2, TiO_2, ZnO, Nb_2O_5, SnO_2, In_2O_3) Films. *J. Phys. Chem. B* **108,** 4818–4822, doi: 10.1021/jp031260g (2004).
11. Look, D. C. *et al.* Electrical properties of bulk ZnO. *Solid State Comm.* **105,** 399–401, doi: 10.1016/s0038-1098(97)10145-4 (1998).
12. Seager, C. H. & Myers, S. M. Quantitative comparisons of dissolved hydrogen density and the electrical and optical properties of ZnO. *J. Appl. Phys.* **94,** 2888–2894, doi: 10.1063/1.1595147 (2003).
13. Gubbala, S., Chakrapani, V., Kumar, V. & Sunkara, M. K. Band-edge engineered hybrid structures for dye-sensitized solar cells based on SnO_2 nanowires. *Adv. Func. Mater.* **18,** 2411–2418, doi: 10.1002/adfm.200800099 (2008).
14. Jarzebski, Z. M. & Marton, J. P. Physical Properties of SnO_2 Materials: II . Electrical Properties. *J. Electrochem. Soc.* **123,** 299C–310C, doi: 10.1149/1.2133090 (1976).
15. Arnold, M. S., Avouris, P., Pan, Z. W. & Wang, Z. L. Field-Effect Transistors Based on Single Semiconducting Oxide Nanobelts. *J. Phys. Chem. B* **107,** 659–663, doi: 10.1021/jp0271054 (2002).
16. Shang, G. *et al.* Preparation of hierarchical tin oxide microspheres and their application in dye-sensitized solar cells. *J. Mater. Chem.* **22,** 25335–25339, doi: 10.1039/C2JM33897A (2012).
17. Fonstad, C. G. & Rediker, R. H. Electrical Properties of High-Quality Stannic Oxide Crystals. *J. Appl. Phys.* **42,** 2911–2918, doi: http://dx.doi.org/10.1063/1.1660648 (1971).
18. Duan, Y. *et al.* Enhancing the performance of dye-sensitized solar cells: doping SnO_2 photoanodes with Al to simultaneously improve conduction band and electron lifetime. *J. Mater. Chem. A* **3,** 3066–3073, doi: 10.1039/C4TA05923A (2015).
19. Wali, Q. *et al.* Multiporous nanofibers of SnO_2 by electrospinning for high efficiency dye-sensitized solar cells. *J. Mater. Chem. A* **2,** 17427–17434, doi: 10.1039/C4TA03056G (2014).
20. Dong, Z. *et al.* Quintuple-Shelled SnO_2 Hollow Microspheres with Superior Light Scattering for High-Performance Dye-Sensitized Solar Cells. *Adv. Mater.* **26,** 905–909, doi: 10.1002/adma.201304010 (2014).
21. Ansari, S. G., Gosavi, S. W., Gangal, S. A., Karekar, R. N. & Aiyer, R. C. Characterization of SnO_2-based H_2 gas sensors fabricated by different deposition techniques. *J. Mater. Sci.: Mater. El.* **8,** 23–27, doi: 10.1023/a:1018544702391 (1997).
22. Ansari, S. G. *et al.* Effect of thickness on H_2 gas sensitivity of SnO_2 nanoparticle-based thick film resistors. *J. Mater. Sci. Mater. El.* **7,** 267–270, doi: 10.1007/bf00188953 (1996).
23. Ansari, S. A., Khan, M. M., Ansari, M. O., Lee, J. & Cho, M. H. Visible light-driven photocatalytic and photoelectrochemical studies of Ag-SnO_2 nanocomposites synthesized using an electrochemically active biofilm. *RSC Adv.* **4,** 26013–26021, doi: 10.1039/C4RA03448A (2014).
24. Ansari, S. A., Khan, M. M., Omaish Ansari, M., Lee, J. & Cho, M. H. Highly photoactive SnO_2 nanostructures engineered by electrochemically active biofilm. *New J. Chem.* **38,** 2462–2469, doi: 10.1039/C3NJ01488F (2014).
25. Green, A. N. M., Palomares, E., Haque, S. A., Kroon, J. M. & Durrant, J. R. Charge Transport versus Recombination in Dye-Sensitized Solar Cells Employing Nanocrystalline TiO_2 and SnO_2 Films. *J. Phys. Chem. B* **109,** 12525–12533, doi: 10.1021/jp050145y (2005).

26. Qian, J. *et al.* TiO₂-Coated Multilayered SnO₂ Hollow Microspheres for Dye-Sensitized Solar Cells. *Adv. Mater.* **21,** 3663–3667, doi: 10.1002/adma.200900525 (2009).
27. Kay, A. & Grätzel, M. Dye-Sensitized Core−Shell Nanocrystals: Improved Efficiency of Mesoporous Tin Oxide Electrodes Coated with a Thin Layer of an Insulating Oxide. *Chem. Mater.* **14,** 2930–2935, doi: 10.1021/cm0115968 (2002).
28. Zhu, K., Schiff, E. A., Park, N.-G., van de Lagemaat, J. & Frank, A. J. Determining the locus for photocarrier recombination in dye-sensitized solar cells. *Appl. Phys. Lett.* **80,** 685–687, doi: http://dx.doi.org/10.1063/1.1436533 (2002).
29. Fabregat-Santiago, F., Bisquert, J., Garcia-Belmonte, G., Boschloo, G. & Hagfeldt, A. Influence of electrolyte in transport and recombination in dye-sensitized solar cells studied by impedance spectroscopy. *Sol. Ener. Mater. Sol. Cells* **87,** 117–131, doi: http://dx.doi.org/10.1016/j.solmat.2004.07.017 (2005).
30. Kim, Y. J. *et al.* Effect of Layer-by-Layer Assembled SnO₂ Interfacial Layers in Photovoltaic Properties of Dye-Sensitized Solar Cells. *Langmuir* **28,** 10620–10626, doi: 10.1021/la3015699 (2012).
31. Wang, Q. *et al.* Characteristics of High Efficiency Dye-Sensitized Solar Cells. *J. Phys. Chem. B* **110,** 25210–25221, doi: 10.1021/jp064256o (2006).
32. Fabregat-Santiago, F., Garcia-Belmonte, G., Mora-Sero, I. & Bisquert, J. Characterization of nanostructured hybrid and organic solar cells by impedance spectroscopy. *Phys. Chem. Chem. Phys.* **13,** 9083–9118, doi: 10.1039/C0CP02249G (2011).
33. Ito, S. *et al.* Control of dark current in photoelectrochemical (TiO₂/I–I³⁻) and dye-sensitized solar cells. *Chem. Comm.* **34,** 4351–4353, doi: 10.1039/B505718C (2005).
34. Snaith, H. J. & Ducati, C. SnO₂-Based Dye-Sensitized Hybrid Solar Cells Exhibiting Near Unity Absorbed Photon-to-Electron Conversion Efficiency. *Nano Lett.* **10,** 1259–1265, doi: 10.1021/nl903809r (2010).
35. Liu, Z. *et al.* The performances of the mercurochrome-sensitized composite semiconductor photoelectrochemical cells based on TiO₂/SnO₂ and ZnO/SnO₂ composites. *Thin Solid Films* **468,** 291–297, doi: http://dx.doi.org/10.1016/j.tsf.2004.05.033 (2004).
36. Gust, D., Moore, T. A. & Moore, A. L. Mimicking Photosynthetic Solar Energy Transduction. *Acc. Chem. Res.* **34,** 40–48, doi: 10.1021/ar9801301 (2000).
37. Gracia, F., Holgado, J. P. & González-Elipe, A. R. Photoefficiency and Optical, Microstructural, and Structural Properties of TiO₂ Thin Films Used as Photoanodes. *Langmuir* **20,** 1688–1697, doi: 10.1021/la034998y (2004).
38. Hagfeldt, A. *et al.* A system approach to molecular solar cells. *Coord. Chem. Rev.* **248,** 1501–1509, doi:http://dx.doi.org/10.1016/j.ccr.2004.04.012 (2004).
39. Gregg, B. A. Interfacial processes in the dye-sensitized solar cell. *Coord. Chem. Rev.* **248,** 1215–1224, doi: http://dx.doi.org/10.1016/j.ccr.2004.02.009 (2004).
40. Gregg, B. A. Excitonic Solar Cells. *J. Phys. Chem. B* **107,** 4688–4698, doi: 10.1021/jp022507x (2003).
41. Grant, C. D. *et al.* Characterization of nanocrystalline and thin film TiO₂ solar cells with poly(3-undecyl-2,2′-bithiophene) as a sensitizer and hole conductor. *J. Electroanal. Chem.* **522,** 40–48, doi: http://dx.doi.org/10.1016/S0022-0728(01)00715-X (2002).
42. Gu, F. *et al.* Improved photoelectric conversion efficiency from titanium oxide-coupled tin oxide nanoparticles formed in flame. *J. Power Sources* **268,** 922–927, doi: http://dx.doi.org/10.1016/j.jpowsour.2014.06.012 (2014).
43. Barbé, C. J. *et al.* Nanocrystalline Titanium Oxide Electrodes for Photovoltaic Applications. *J. Amer. Cer. Soc.* **80,** 3157–3171, doi: 10.1111/j.1151-2916.1997.tb03245.x (1997).
44. Zhong, M., Shi, J., Zhang, W., Han, H. & Li, C. Charge recombination reduction in dye-sensitized solar cells by depositing ultrapure TiO₂ nanoparticles on "inert" BaTiO₃ films. *Mater. Sci. Eng. B* **176,** 1115–1122, doi: http://dx.doi.org/10.1016/j.mseb.2011.05.052 (2011).
45. Weiwei, X. *et al.* Influence of Different Surface Modifications on the Photovoltaic Performance and Dark Current of Dye-Sensitized Solar Cells. *Plasma Science and Tech.* **9,** 556–559, doi: 10.1088/1009-0630/9/5/08. (2007).
46. Lee, S.-W., Ahn, K.-S., Zhu, K., Neale, N. R. & Frank, A. J. Effects of TiCl₄ Treatment of Nanoporous TiO₂ Films on Morphology, Light Harvesting, and Charge-Carrier Dynamics in Dye-Sensitized Solar Cells. *J. Phys. Chem. C* **116,** 21285–21290, doi: 10.1021/jp3079887 (2012).
47. O'Regan, B. C., Durrant, J. R., Sommeling, P. M. & Bakker, N. J. Influence of the TiCl₄ Treatment on Nanocrystalline TiO₂ Films in Dye-Sensitized Solar Cells. 2. Charge Density, Band Edge Shifts, and Quantification of Recombination Losses at Short Circuit. *J. Phys. Chem. C* **111,** 14001–14010, doi: 10.1021/jp073056p (2007).
48. Cameron, P. J., Peter, L. M. & Hore, S. How important is the back reaction of electrons via the substrate in dye-sensitized nanocrystalline solar cells? *J. Phys. Chem. B* **109,** 930–9366, doi: 10.1021/jp0405759 (2005).
49. Yoo, B. *et al.* Chemically deposited blocking layers on FTO substrates: Effect of precursor concentration on photovoltaic performance of dye-sensitized solar cells. *J. Electroanal. Chem.* **638,** 161–166, doi: 10.1016/j.jelechem.2009.10.005 (2010).
50. Goes, M. S. *et al.* Impedance Spectroscopy Analysis of the Effect of TiO₂ Blocking Layers on the Efficiency of Dye Sensitized Solar Cells. *J. Phys. Chem. C* **116,** 12415–12421, doi: 10.1021/jp301694r (2012).
51. Fabregat-Santiago, F. *et al.* Correlation between photovoltaic performance and impedance spectroscopy of dye-sensitized solar cells based on ionic liquids. *J. Phys. Chem. C* **2,** 6550–6560, doi: 10.1021/jp066178a (2007).
52. Wang, Q., Moser, J.-E. & Grätzel, M. Electrochemical impedance spectroscopic analysis of dye-sensitized solar cells. *J. Phys. Chem. B* **109,** 14945–14953, doi: 10.1021/jp052768h (2005).
53. Bisquert, J. Theory of the Impedance of Electron Diffusion and Recombination in a Thin Layer. *J. Phys. Chem. B* **106,** 325–333, doi: 10.1021/jp011941g (2002).
54. Bisquert, J., Mora-Sero, I. & Fabregat-Santiago, F. Diffusion-Recombination Impedance Model for Solar Cells with Disorder and Nonlinear Recombination. *ChemElectroChem* **1,** 289–296, doi: 10.1002/celc.201300091 (2014).
55. Gregg, B. A., Pichot, F., Ferrere, S. & Fields, C. L. Interfacial Recombination Processes in Dye-Sensitized Solar Cells and Methods To Passivate the Interfaces. *J. Phys. Chem. B* **105,** 1422–1429, doi: 10.1021/jp003000u (2001).
56. Kavan, L., Tétreault, N., Moehl, T. & Grätzel, M. Electrochemical Characterization of TiO₂ Blocking Layers for Dye-Sensitized Solar Cells. *J. Phys. Chem. C* **118,** 16408–16418, doi: 10.1021/jp4103614 (2014).
57. Selopal, G. S. *et al.* Effect of Blocking Layer to Boost Photoconversion Efficiency in ZnO Dye-Sensitized Solar Cells. *ACS Appl. Mater. & Interf.* **6,** 11236–11244, doi: 10.1021/am501360a (2014).
58. Choi, H. *et al.* The effect of TiCl₄-treated TiO₂ compact layer on the performance of dye-sensitized solar cell. *Curr. Appl. Phys.* **12,** 737–741, doi: 10.1016/j.cap.2011.10.011 (2012).
59. Docampo, P., Ball, J. M., Darwich, M., Eperon, G. E. & Snaith, H. J. Efficient organometal trihalide perovskite planar-heterojunction solar cells on flexible polymer substrates. *Nat. Comm.* **4,** doi: 10.1038/ncomms3761 (2013).
60. Morales, A. E., Mora, E. S. & Pal, U. Use of diffuse reflectance spectroscopy for optical characterization of un-supported nanostructures. *Revista Mexicana de Fisica S* **53,** 18–22 (2007).
61. Chen, W. *et al.* Hybrid interfacial layer leads to solid performance improvement of inverted perovskite solar cells. *En. & Env. Sci.* **8,** 629–640, doi: 10.1039/C4EE02833C (2015).
62. Cariello, M. *et al.* An investigation of the role increasing [small pi]-conjugation has on the efficiency of dye-sensitized solar cells fabricated from ferrocene-based dyes. *RSC Adv.* **6,** 9132–9138, doi: 10.1039/C5RA21565J (2016).
63. Zhang, J. *et al.* Energy barrier at the N719-dye/CsSnI₃ interface for photogenerated holes in dye-sensitized solar cells. *Sci. Rep.* **4,** 6954, doi: 10.1038/srep06954 (2014).

Author Contributions

K.B. designed the device optimization strategy, fabricated and characterized the devices. K.B. and H.Z. analysed the results. D.B. carried out EIS experiments, analysed the results and provided their interpretation. L.J. carried out XPS experiments. H.Z., A.V., F.V. and F.R. supervised the experiments. A.V. and F.R. designed the project. K.B. wrote the manuscript. H.Z., A.V., F.V. and F.R. reviewed and corrected the manuscript. All the authors participated in the discussion and commented on the paper.

Additional Information

Supplementary information accompanies this paper at http://www.nature.com/srep

Competing financial interests: The authors declare no competing financial interests.

How to cite this article: Basu, K. *et al.* Enhanced photovoltaic properties in dye sensitized solar cells by surface treatment of SnO$_2$ photoanodes. *Sci. Rep.* **6**, 23312; doi: 10.1038/srep23312 (2016).